J Mol Model (2013) 19:5343–5354
DOI 10.1007/s00894-013-2021-7

ORIGINAL PAPER

Electronic, ductile, phase transition and mechanical properties of Lu-monopnictides under high pressures

Dinesh C. Gupta · Idris Hamid Bhat

Received: 24 July 2013 / Accepted: 22 September 2013 / Published online: 26 October 2013

Abstract The structural, elastic and electronic properties of lutatium-pnictides (LuN, LuP, LuAs, LuSb, and LuBi) were analyzed by using full-potential linearized augmented plane wave within generalized gradient approximation in the stable rock-salt structure (B1 phase) with space group Fm-3m and high-pressure CsCl structure (B2 phase) with space group Pm-3m. Hubbard-U and spin-orbit coupling were included to predict correctly the semiconducting band gap of LuN. Under compression, these materials undergo first-order structural transitions from B1 to B2 phases at 241, 98, 56.82, 25.2 and 32.3 GPa, respectively. The computed elastic properties show that LuBi is ductile by nature. The electronic structure calculations show that LuN is semiconductor at ambient conditions with an indirect band gap of 1.55 eV while other Lu-pnictides are metallic. It was observed that LuN shows metallization at high pressures. The structural properties, viz, equilibrium lattice constant, bulk modulus and its pressure derivative, transition pressure, equation of state, volume collapse, band gap and elastic moduli, show good agreement with available data.

Keywords Phase transition · Band structure · Heavy rare-earth · Mono-pnictides · Lattice constant · Elastic moduli

D. C. Gupta (✉) · I. H. Bhat
Condensed Matter Theory Group, School of Studies in Physics, Jiwaji University, Gwalior 474 011, India
e-mail: sosfizix@yahoo.co.in

I. H. Bhat
e-mail: idu.idris@gmail.com

I. H. Bhat
e-mail: dcgupta@jiwaji.edu

Introduction

In recent years, the study of cohesive, structural phase transformation, electronic, thermal, mechanical and magnetic properties of binary rare earth (RE) monopnictides have received considerable attention. The subject of interest remains their occupation numbers in the shallow inner 4*f* shell, ranging from 0 to 14 through the series La to Lu. The 4*f* occupation confers a wide range of electronic and magnetic properties on these RE elements and their compounds [1], despite their NaCl structure (B1 Phase). The 4*f* electrons are usually considered to be highly localized in these compounds thus present a challenging problem to obtain accurate theoretical descriptions of the electronic structures [2]. The 4*f*–5*d* interactions and the hybridizations between rare-earth non-4*f* and pnictogen *p* states are responsible for the many interesting phenomena that occur in these RE monopnictides. Further, the bonding between the RE and pnictogen atoms cannot simply be described as ionic or covalent, otherwise they would all be expected to be insulators (semiconductors) [3]. High pressure studies of these materials reveal that the majority of the compounds undergo a first-order structural phase transition from the NaCl (B1 phase) structure with space group Fm-3m to CsCl structure (B2 phase) with space group Pm-3m. The crystal structure properties of RE-pnictides have been investigated by using a high pressure X-ray diffraction technique [4–7]. In addition to experimental work, theoretical studies based on density functional theory (DFT) have also verified experimental results successfully and have been useful in predicting interesting properties that are yet to be explored experimentally. Various theoretical studies of the electronic structure of RE pnictides have been predicted in detail [8, 9], Gd-monopnictides are the most extensively RE studied

theoretically. These are the simplest series because of Gd being located in the center of the RE metal series and having half-filled 4*f* electrons. These materials show unusual electric [10] and magnetic [11, 12] phenomena. Their electronic structure and transport properties remain controversial. Calculations of these materials were also reported within local-spin density approximation (LSDA) [13, 14]. Later studies were also performed to investigate CeSb [15], DyBi, and DyP [16].

Lutatium-pnictides (Lu-X; X = N, P, As, Sb, and Bi) are the least studied among RE-materials. Being the last and heaviest member of the lanthanide-series with a completely filled 4*f* shell, Lu has been least studied of all. The central focus of the present study was to investigate the less studied Lu-pnictides at ambient pressure as well as under high pressure. High-pressure studies are important because little information on Lu-pnictides under high pressures is available in the literature. A proper understanding of the effect of high-pressures on the electronic structure of these materials was also a central focus of the present study. Shirotani et al. [5] reported the high pressure structural phase transition of Lu-monopnictides (LuAs and LuSb) using a powder X-ray diffraction technique. Recently, Pagare et al. [17] reported the theoretical electronic structure of LuAs and LuSb along with elastic and phase transition properties using DFT. Despite a little theoretical study on LuN, LuP and LuBi [18] and the high pressure experimental study of LuP [19], no more data are available on the electronic and high pressure phase transition properties for LuN, LuP and LuBi compounds. The main aim of the present work was to perform a comprehensive study of Lu-monopnictides and to investigate the high-pressure behavior of these materials along with their elastic properties. Further, electronic and thermal properties are also reported for the first time for LuN, LuP and LuBi using effective on-site coulomb potential. The present study is important because it reports for the first time the band structure of semiconducting LuN with the correct value of band-gap along with LuP and LuBi. A comparison between GGA and GGA + U + SO was also performed in the present study to report the correct approach to investigation of the electronic properties of the present materials. The LDA, LSDA and LSDA + U were also tried, but the values of material properties were quite far away from the measured data, particularly the band gap value of LuN.

The computational methods and the parameters used are described in the next section. The Results and discussion deals with the calculated results on structural, electronic and elastic properties of Lu-monopnictides, discussed in the light of available data. A final Conclusions summarizes the findings and draws attention to some of the most interesting predictions.

Computational methods

All computations were performed using a first-principles full-potential linearized augmented plane wave method (FP-LAPW) as implemented in the Wien2k package [20, 21]. The generalized gradient approximation (GGA) [22] was chosen for the exchange-correlation potential. Spin-polarized calculations were carried out with both majority-spin and minority-spin states. It was found that band structure shows a metallic character in all the cases while LuN is semiconductor by nature. To obtain the exact nature of the electronic structure, we used GGA + Hubbard-U (on-site coulomb interaction) method [23, 24]. In GGA + U-like methods, an orbitally dependent potential is introduced for the chosen set of electronic states, which are 5*d* states of Lu in the present case. This additional potential has an atomic Hartree-Fock (HF) form but with screened Coulomb and exchange interaction parameters. The coulomb potential U=6.48 eV and the exchange coupling J= 2.05 eV, i.e., the effective on-site term (U − J) is 4.44 eV for the Lu 5*d* orbitals has been calculated in the super-cell approximation using this method [25]. The fully localized limit version of the GGA + U method was employed. Spin-orbit coupling (SOC) was included because of the second variational method using a scalar relativistic wave functions [21]. Inside the non-overlapping spheres of muffin-tin radius R_{MT}, the linear combination of radial solution of the Schrödinger equation times the spherical harmonics is used, whereas the plane basis set is chosen in the interstitial region. R_{MT} is chosen in such a way that there is no charge leakage from the core and total energy convergence is ensured. Further, for energy Eigen-value convergence, the wave function in the interstitial region is expanded in terms of plane waves with a cut-off parameter $K_{MAX}R_{MT}=8.5$, where K_{MAX} is the maximum value of the reciprocal lattice vector used in the plane wave expansion, and R_{MT} is the smallest atomic-sphere radius of all the atomic spheres. The maximum value of angular momentum $l_{MAX}=10$ is taken for the wave function expansion inside the atomic spheres. In the interstitial region the charge density and the potential were expanded as a Fourier series with wave vectors up to $G_{MAX}=12$ a.u.$^{-1}$. We have used a dense mesh of 1,000 k-points (4,000 k-points for LuN) and the tetrahedral method [26] was employed for Brillouin zone (BZ) integration. The self-consistent calculations were considered to converge only when the calculated total energy of the crystal converges to less than 10^{-4} Ry.

The total energies were further used to obtain the ground state properties. The elastic constants are very important as they are related to numerous fundamental

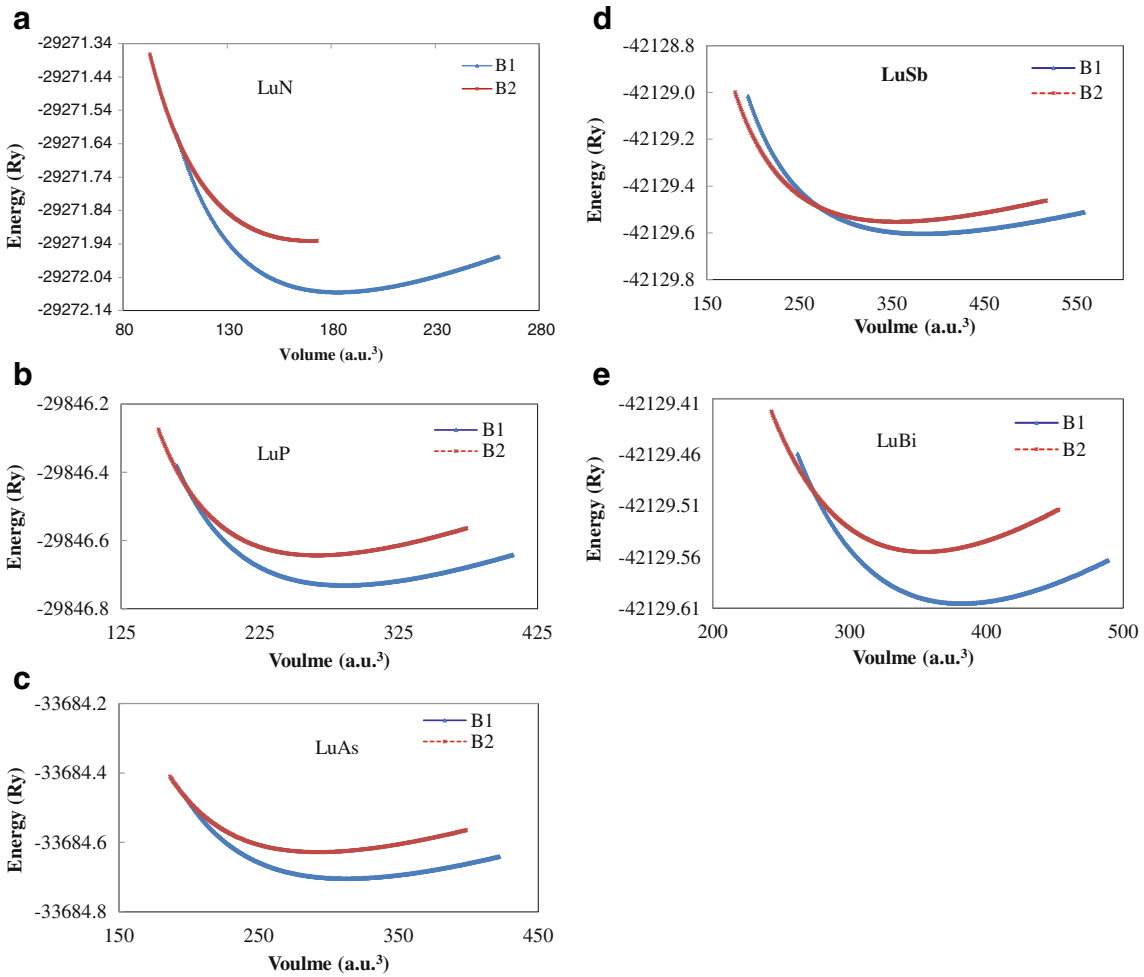

Fig. 1 Total energy vs cell volume in B1 and B2 phases of **a** LuN, **b** LuP, **c** LuAs, **d** LuSb, **e** LuBi

properties of solids. Thermodynamic properties, like, specific heat, thermal expansion, Debye temperature can also be predicted as these properties are linked to elastic constants. In the present study, the method as integrated in Wien2k was used to calculate elastic constants [21]. The transverse and longitudinal sound velocities (v_t and v_l) were obtained using the following combinations of elastic constants:

Table 1 The values of lattice parameter (a in Å), bulk modulus (B_o in GPa) and its pressure derivative (B_o') of Lu-pnictides in B1 and B2 phases

Solids	B1 Phase			B2 Phase			Study
	a	B_0	B_0'	a	B_0	B_0'	
LuN	4.77	164.07	3.81	2.93	179.44	3.45	Present
	4.77	–	–	–	–	–	Experimental [30]
LuP	5.53	87.24	3.57	3.40	88.93	3.87	Present
	5.53	–	–	–	–	–	Experimental [30]
LuAs	5.68	81.02	3.77	3.51	84.25	3.86	Present
	5.68	85±3	5.90	–	–	–	Experimental [5]
	5.68	82.40	3.97	3.50	85.30	4.07	Others [17]
LuSb	6.09	60.69	3.82	3.74	63.77	3.49	Present
	6.04	53±4	6±0.8				Experimental [5]
	6.11	58.04	3.75	3.72	66.40	4.11	Others [17]
LuBi	6.24	54.08	3.95	3.85	55.83	3.62	Present
	6.16	–	–	–	–	–	Experimental [30]

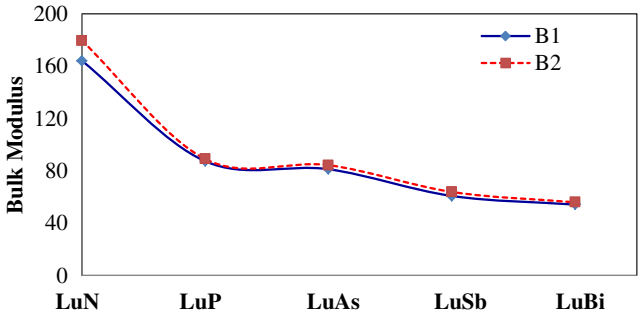

Fig. 2 Variation in bulk modulus (in GPa) with increasing size of pnictogen atom of Lu-pnictides in B1 phase

$$v_t = \left[\frac{C_{44} - 0.2(2C_{44} + C_{12} - C_{11})}{\rho}\right]^{\frac{1}{2}}$$

and

$$v_l = \left[\frac{C_{11} + 0.4(2C_{44} + C_{12} - C_{11})}{\rho}\right]^{\frac{1}{2}}$$

Here C_{11}, C_{12} and C_{44} are second-order elastic constants (SOECs) with ρ as mass density per unit volume. The average sound velocity v_m is calculated as [27, 28]:

$$v_m = \left[\frac{1}{3}\left(\frac{2}{v_t^3} + \frac{1}{v_l^3}\right)\right]^{-1/3}$$

In order to calculate Debye temperature, we have used the fundamental equation [27, 29]:

$$\theta_D = \frac{h}{k_B}\left(\frac{3n}{4\pi V_a}\right)^{\frac{1}{3}} v_m$$

where h is Plank's constant, k_B is Boltzmann's constant, n is number of atoms/f.u. and V_a is the average atomic volume.

Results and discussion

Structural properties

In order to calculate the ground state properties of the present set of materials, the total energy of the system was calculated at different volumes, with the equilibrium corresponding to the lowest value of the total energy. Plots of total energy as a function of volume were fitted to Murnaghan's equation of state and plotted in Fig. 1a–e for B1 and B2 phases. The present calculations show that the ground state configuration of all these materials lies in a rock-salt (B1) structure, which is consistent with experimental [5, 30, 31] and other theoretical [17] results. Using these minimization curves, ground state properties like equilibrium lattice constant (a), bulk modulus (B_0) and its first-order pressure derivative were calculated. The results are reported in Table 1 together with the other

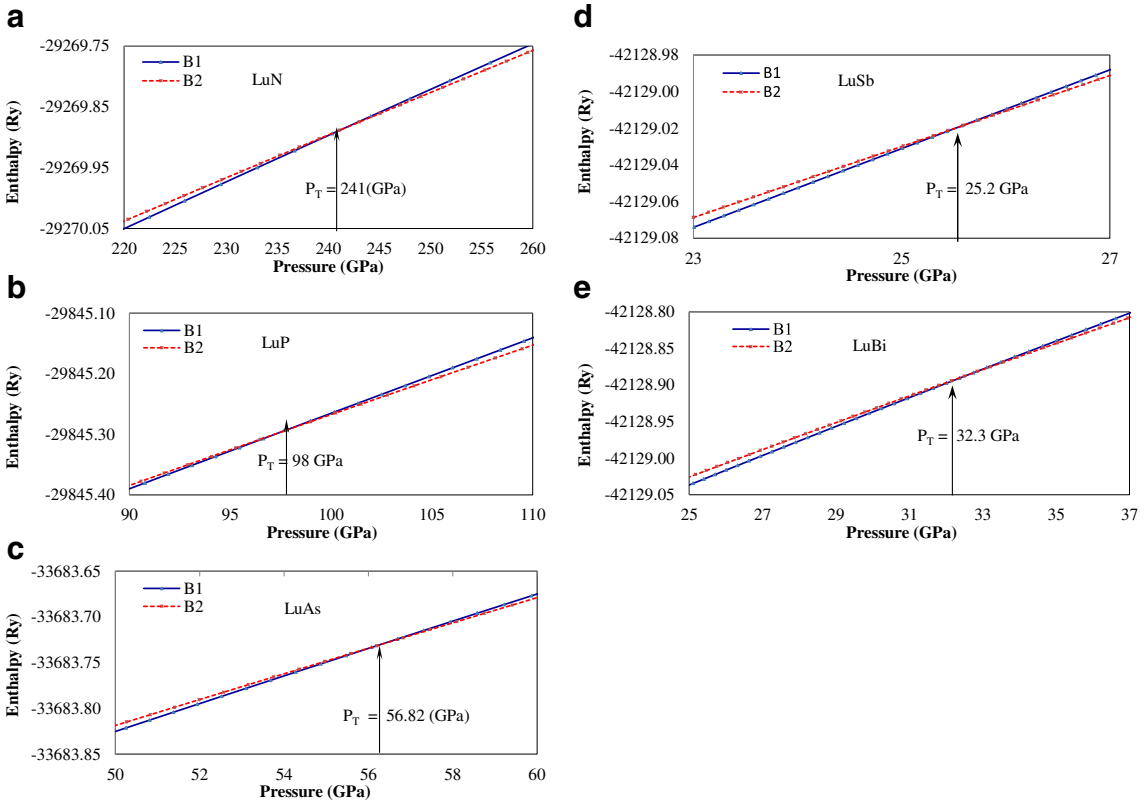

Fig. 3 Enthalpy vs pressure in B1 and B2 phases of. **a** LuN, **b** LuP, **c** LuAs, **d** LuSb, **e** LuBi

Table 2 Calculated values of the phase transition pressure (P_T in GPa), the percentage volume collapse at P_T [$\Delta V(P_T)/V(0)$] and the change in the enthalpy ($\Delta H = H_{B2} - H_{B1}$ in Ry) for Lu-pnictides

Solids	ΔH	P_T	$\%\Delta V(P_T)/V(0)$	Work
LuN	0.15	241.0	5.0	Present
LuP	0.09	98.0	7.2	Present
LuAs	0.07	56.82	3.4	Present
	–	57.0	–	Experimental [5]
		56.7	3.0	Others [17]
LuSb	0.05	25.2	1.0	Present
	–	24.0	1.0	Experimental [31]
	–	25.2	5.0	Others [17]
LuBi	0.05	32.3	5.4	Present

results. The calculated values of a and B_0 are in reasonable agreement with experimental data. The variation in the bulk modulus of these materials is plotted as a function of increasing size of pnictogen atom in Fig. 2 to obtain the compressibility behavior. It is clear from Fig. 2 that the bulk modulus decreases from LuN to LuBi, indicating the increasing trend of compressibility with increasing size of pnictogen atom.

To determine the structural stability at finite pressure and temperature for B1 and B2 phases, we used enthalpy $H = E_{Total} + PV$ at T=0 K. The enthalpies corresponding to both the phases are equal at phase transition pressure (P_T). The variation of enthalpy as a function pressure is plotted in Fig. 3a–e. It may be seen that the enthalpy in parent (B1) phase is minimum at ambient conditions and remains minimum up to 241, 98, 56.82, 25.2 and 32.3 GPa for LuN, LuP, LuAs, LuSb, and LuBi, respectively. The enthalpies in both phases become equal, showing that both phases are in equilibrium at this pressure (P_T), and hence structural phase transformation occurs in Lu-pnictides at this point. On further increasing the pressure, the enthalpy minimizes in B2 phase as compared to that of B1 phase, i.e., the B2 phase becomes

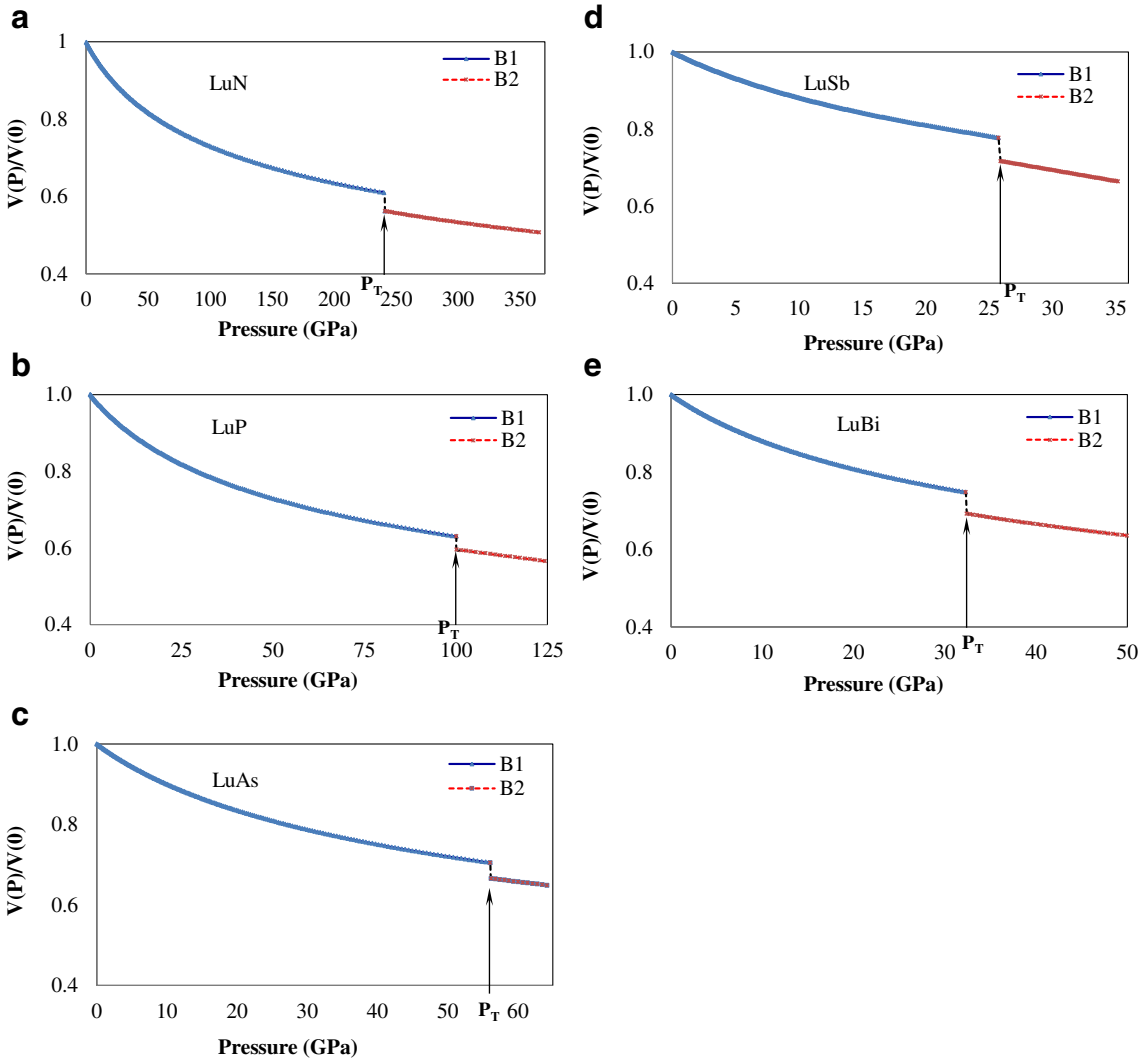

Fig. 4 Equation of state/phase diagram of **a** LuN, **b** LuP, **c** LuAs, **d** LuSb, **e** LuBi

Table 3 Calculated values of elastic properties (in GPa), and A, B/G and ξ are dimensionless for Lu-pnictides in B1 phase

Property	LuN	LuP	LuAs	LuSb	LuBi	Work
C_{11}	358.43	212.86	197.47	147.64	118.14	Present
	–	–	183.38	122.36	–	Others [17]
C_{12}	76.93	24.43	22.80	18.63	21.21	Present
	–	–	31.85	25.89	–	Others [17]
C_{44}	143.80	53.54	38.87	25.96	10.72	Present
	–	–	61.48	21.37	–	Others [17]
C_S	140.75	94.22	87.34	64.51	48.47	Present
C_L	361.48	172.19	149.01	109.10	80.40	Present
G	142.58	69.81	58.26	41.38	25.82	Present
E	334.61	165.33	140.98	101.43	66.72	Present
μ	142.58	69.81	58.26	41.38	25.82	Present
λ	75.71	40.70	42.19	34.05	36.31	Present
ξ	0.37	0.27	0.27	0.28	0.33	Present
C_{12}–C_{44}	−66.87	−29.11	−16.07	−7.33	10.49	Present
A	1.02	0.57	0.45	0.40	0.22	Present
B_0/G	1.20	1.25	1.39	1.49	2.07	Present

stable with minimum enthalpy. The values of enthalpies in B1 and B2 phases have been used to compute the difference of enthalpies $\Delta H = H_{B2} - H_{B1}$. These values of ΔH and phase transition pressure (P_T) are reported in Table 2. The equations of state plotted in Fig. 4a–e for Lu-pnictides were used to compute the volume collapse [$\Delta V(P_T)/V(0)$] at P_T. These values are also included in Table 2 along with measured [5] and other theoretical [17] data. It is clear from Fig. 4a that the volume of LuN decreases smoothly up to 241 GPa. An abrupt decline in volume is observed at this pressure, which is associated with a structural phase transformation from B1→B2 phase and thereafter no other transformation is observed because no abrupt decline in volume is found up to 400 GPa in few other structures. Similar trend of transformations are found in other lutetium-pnictide compounds as shown in Fig. 4b–e, except that the transition occurs at different magnitude of pressure, i.e., 98, 56.82, 25.2 and 32.3 GPa,

Table 4 Calculated values of the longitudinal, transverse and average sound velocity (v_l, v_t and v_m in m/s) and Debye temperature (θ_D in K) for Lu-pnictides in B1 phase

Solids	v_l	v_t	v_m	θ_D	Work
LuN	5,586.26	3,511.36	3,865.70	482.49	Present
LuP	4,721.89	2,938.01	3,238.07	348.61	Present
LuAs	4,186.11	2,536.27	2,803.03	293.81	Present
	4,359.00	2,725.00	2,999.00	309.00	Others [17]
LuSb	3,658.90	2,177.74	2,410.98	235.70	Present
	3,419.00	1,929.00	2,144.00	205.00	Others [17]
LuBi	2,894.80	1,568.47	1,750.23	166.99	Present

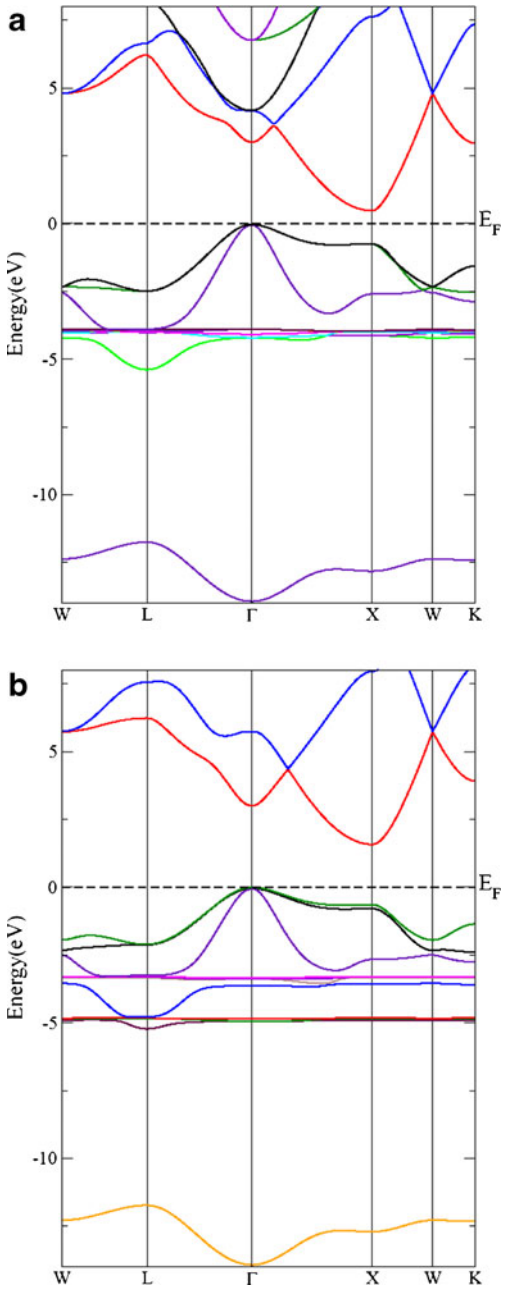

Fig. 5 Band structure of LuN in B1 phase at ambient conditions for **a** GGA + U and **b** GGA + U + SO

respectively, in LuP, LuAs, LuSb abs LuBi. The percentage values of the discontinuities in reduced volume at P_T [$\Delta V(P_T)/V(0)$] are also reported in Table 2 along with available data.

Elastic properties

Acquaintance with the elastic properties of materials promotes understanding of the fundamental aspects of mechanical deformation and the structural properties of crystals, and hence plays an important role in providing valuable information

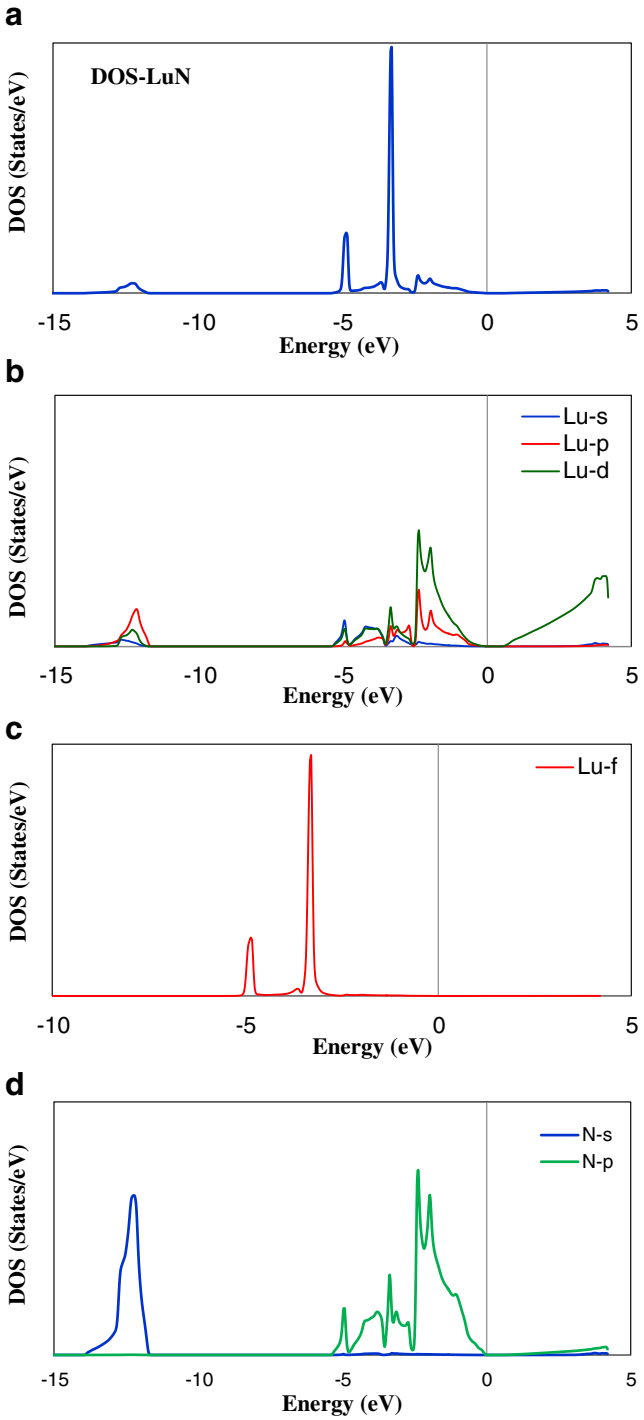

Fig. 6a–d Density of states (DOS) and *l*-projected DOS of LuN for GGA + U + SO in B1 phase at ambient conditions. **a** DOS, **b** partial DOS (PDOS) of Lu (*s*, *p*, and *d* states), **c** PDOS of Lu (*f* states), **d** PDOS of N (*s* and *p* states)

about the binding characteristics between adjacent planes of atoms. Based on elastic properties, anisotropic character of binding and structural stability can also be predicted. In the present study, due to cubic symmetry, the materials have only three independent elastic parameters (C_{11}, C_{12} and C_{44}), which, along with other properties, are calculated and reported in Table 3 and compared with available experimental and other theoretical values.

It can be seen from Table 3 that the unidirectional elastic constant C_{11}, related to the unidirectional compression along the principal crystallographic direction, is higher than C_{44} in every case, indicating that these materials present a weaker resistance to pure shear deformation compared to resistance to unidirectional compression.

For cubic crystals, the necessary condition of existence in a stable or meta-stable phase depends on the mechanical stability criteria [32, 33] $C_{11}>0$; $C_{12}>0$; $C_{11}-C_{12}>0$; $C_{11}+2C_{12}>0$. Computed values of the elastic constants for Lu-pnictides satisfy all the required conditions and hence these materials are mechanically stable in B1 phase.

The elastic anisotropy of crystals, which is highly correlated with the possibility of inducing micro-cracks into materials, has important implications for engineering science. We calculated the elastic anisotropy factor A $\{A=2C_{44}/(C_{11}-C_{12})\}$ from the set of elastic constants [34]. For a material that is completely isotropic, A equals 1, otherwise material is anisotropic. The magnitude of the deviation from 1 is the measure of the degree of elastic anisotropy. The calculated values A for Lu-pnictides are listed in Table 3 and shows the anisotropic nature of these materials. We also calculated the shear modulus and Young's modulus. The shear modulus of a crystal is a measure of the resistance to reversible deformation upon shear stress and is an important factor to predict the hardness rather than bulk modulus. Another quantity used to characterize materials is Young's modulus E. The materials with higher value of E are found to be stiffer than those with lower E values. Hence, based on the present study we can conclude that the stiffness of Lu-pnictides decrease when we move from N to Bi.

There are many other factors that are very useful when investigating the ductile and brittle nature of materials, among them Cauchy's pressure $C_{12}-C_{44}$=2P and Pugh's index of ductility ,which is the ratio of G and B_0, i.e. (B/G), where $G=(C_{11}-C_{12}-3C_{44})/5$.

Cauchy's pressure is the difference between two particular elastic constants ($C_{12}-C_{44}$). The Cauchy's relation is valid only when all inter-atomic forces are composed by two-body central interactions under static lattice conditions. At zero pressure, our calculations give negative values of $C_{12}-C_{44}$ except for LuBi, indicating violation of the Cauchy's relation. The only positive value for LuBi predicts the metallic character of the bonding and rest of the materials are confirmed to have directional bonding (partial covalent) with angular character. The value increases on increasing the size of pnictogen atom in B1 phase, which shows that the non-central character of the forces, implicit in the Cauchy's relation, decreases when the lattice constant increases. The negative value is a consequence of the hybridization of the unstable *f* band [35]. This hybridization may be responsible for the decrease in Lu–Lu distance,

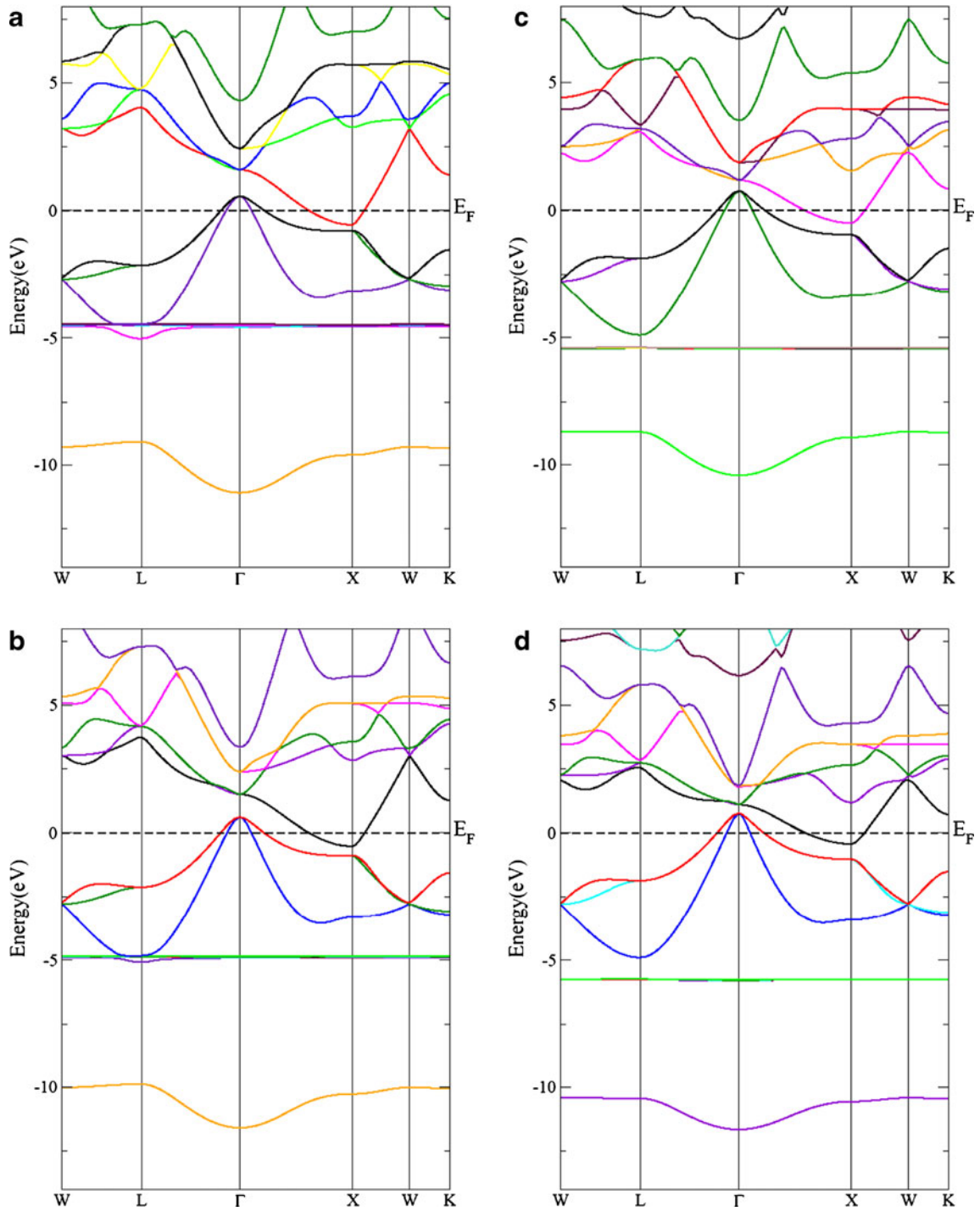

Fig. 7a–d Band structure for GGA + U in B1 phase at ambient conditions. **a** LuP, **b** LuAs, **c** LuSb, **d** LuBi

and thereby the too small value of elastic constant C_{12}. It is also considered to be an indicator of ductility [36]. A material with positive pressure is expected to be ductile and if the pressure is negative, a brittle nature of the material is expected. In case of Lu-pnictides, LuBi has a positive value of pressure, and hence the material is expected to be ductile, while other Lu-pnictides are brittle. Pugh's ratio (B_0/G) is another index that is considered to serve as an indication of ductility. A high B_0/G ratio is associated with ductility whereas a low value corresponds to a brittle nature of materials [37]. The critical value that separates the ductile and brittle nature was found to be 1.75. As shown from Cauchy's pressure, Pugh's index of ductility also predicts the ductile nature of LuBi and brittle character of the remaining compounds of this family in B1 phase.

We also computed the thermo-physical properties of these compounds, i.e., longitudinal, transverse and average sound

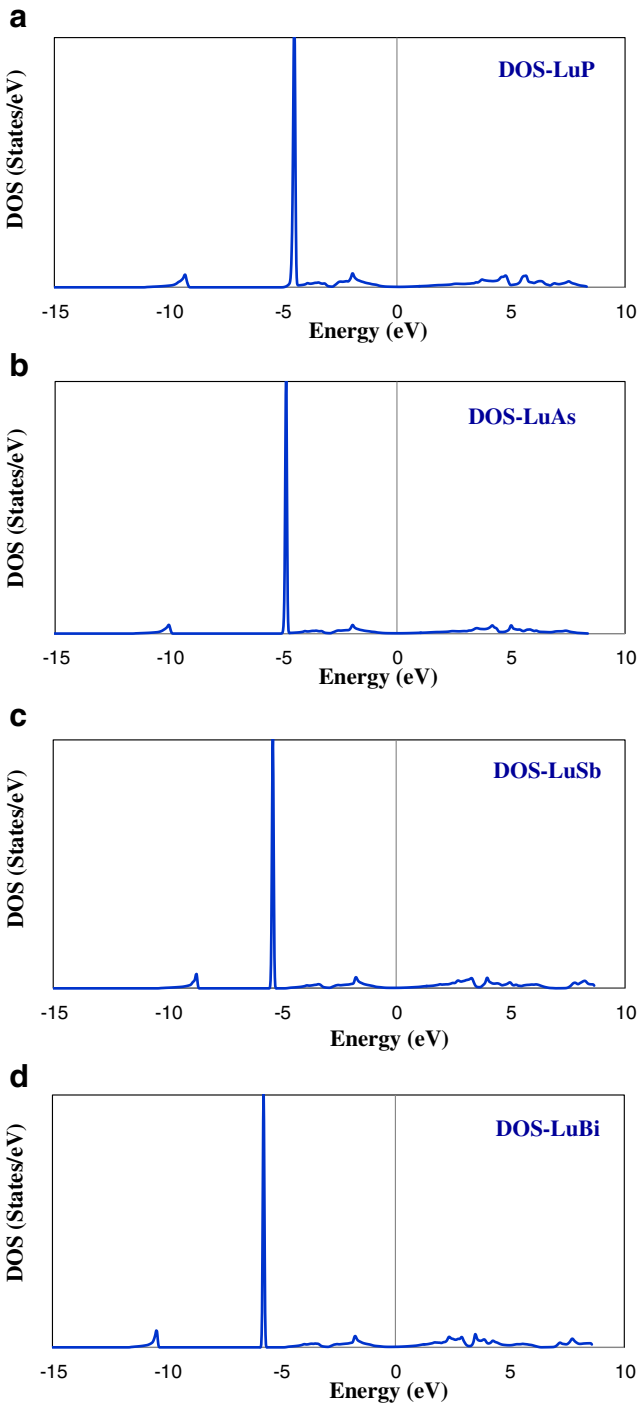

Fig. 8a–d DOS for GGA + U in B1 phase at ambient conditions. **a** LuP, **b** LuAs, **c** LuSb, **d** LuBi

velocities (v_l, v_t, and v_m, respectively), and the Debye temperature, θ_D. These values are reported in Table 4 and compared with other available values. It is clear that the values of θ_D, v_l, v_t and v_m, decrease with the increase of ionic radii of pnictogen atom. In the absence of reported experimental data available in the literature, present values could not be compared. However, our calculated values show good agreement with other theoretical values [17]. Future experimental work will verify these results. We consider the present results as a prediction study for these compounds with the hope that the present work will stimulate further study.

Electronic properties

The electronic structure of Lu-pnictides were studied along the directions of high symmetry in BZ. Figure 5a,b presents the band structure of LuN (in B1 phase) using GGA + U and GGA + (U-J) + SO with Fermi level set at origin. The latter strategy was foudn to have a significant impact on overall band structure, particularly on the energy states near the Fermi level. In Fig. 5a, the top of the valence band (VB) and the bottom of the conduction band (CB) are separated by a band gap of 0.73 eV. However, Fig. 5b shows a clear picture of gap opening when SOC is introduced, though the overall band profile remains similar. The calculated value of the band gap for LuN using the GGA + (U-J) + SO scheme is 1.55 eV, which is in close agreement with the experimental value [30]. The choice of spin polarized GGA + U + SO predicted correctly the band gap and nature of bands as compared to spin polarized GGA, which predicted LuN to be metallic. The electronic structure can be better explained from density of states (DOS), which is reported in Fig. 6a for LuN. A comparison was made by considering DOS and partial density of states (PDOS) in both cases; however, we have reported DOS and PDOS of GGA + (U−J) + SO scheme only. In both schemes, the occupied 4*f* states are located around −4 eV below E_F, strongly hybridized with N 2*p* states; however, a splitting of *f* bands can be observed when SO is introduced. The CB is mainly the contribution of 2p of N around 2–3 eV mixed with Lu 5*d* states around 5 eV. The pnictogen *p* states (here N 2*p*) dominate the top of the valence bands around −2 to −2.5 eV. More precisely, these pnictogen *p* states are actually hybridized with RE Lu-5*d* states around −2 eV, which dominate the bottom of the conduction bands. This hybridization results in a hole pocket at the **Γ** point and an electron pocket at the **X** point in metallic pnictides. The numbers of electrons and holes remain same [14]. Even if the pnictides are semiconductors, the touchdown of the RE 5*d* states at the **X** point would make the energy gap indirect. There is no other theoretical data available for LuN but LuAs and LuSb have been explored theoretically [17]. We compared our results with LuAs and LuSb because LuN belongs to the same family of compounds. In LuAs and LuSb, the bands around −10 eV are due to the *s*-states, bands just below the Fermi level are due to the *p*-states of pnictogen and *d*-states of Lu. Also, the peak above the Fermi level is due to the *d*-states of Lu.

The *l*-projected DOS plot in Fig. 6b–d shows a clearer picture of the electronic structure of LuN. As one can see, the top valence states right below the Fermi level are predominantly N 2*p* states. The Lu *d* states, however, also make a

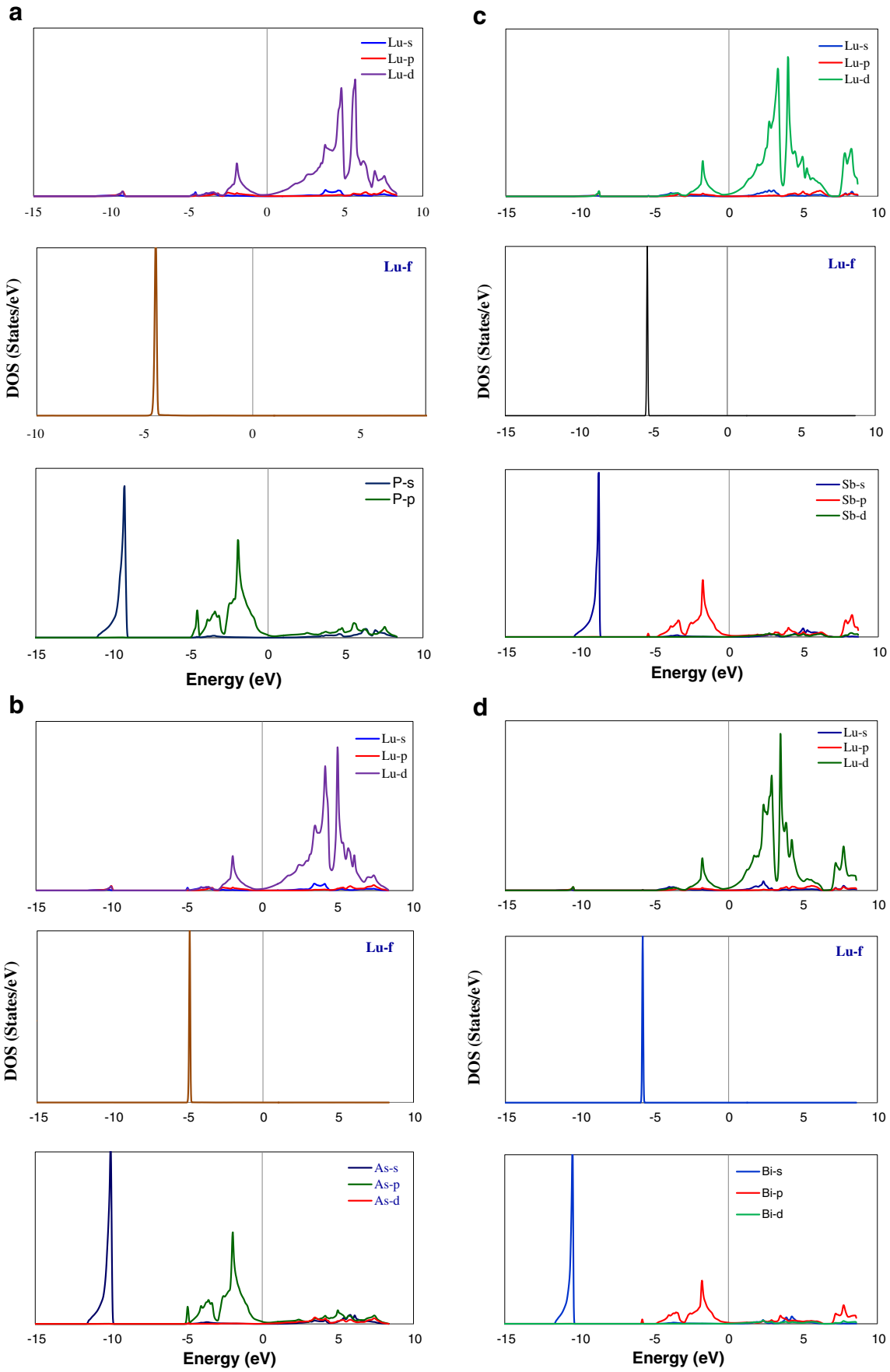
a
Lu-s
Lu-p
Lu-d
Lu-f
DOS (States/eV)
P-s
P-p
Energy (eV)
c
Lu-s
Lu-p
Lu-d
Lu-f
DOS (States/eV)
Sb-s
Sb-p
Sb-d
Energy (eV)
b
Lu-s
Lu-p
Lu-d
Lu-f
DOS (States/eV)
As-s
As-p
As-d
Energy (eV)
d
Lu-s
Lu-p
Lu-d
Lu-f
DOS (States/eV)
Bi-s
Bi-p
Bi-d
Energy (eV)

◀ **Fig. 9a–d** The *l*-projected DOS for GGA + U in B1 phase at ambient conditions. **a** LuP, **b** LuAs, **c** LuSb, **d** LuBi

noticeable contribution. It is noted here that, in our calculations, Lu 5*d* states participate in hybridizations with N 2*p* states, though the bottom of the conduction bands are dominated by 5*d* states. In contrast to the PDOS of GGA + *U* not shown here, the occupied 4*f* bands split further due to spin-orbit coupling. The splitting of 4*f* single peak around −4 eV into two peaks around −4 and −3 eV can be seen in Fig. 6c.

We also calculated the band structures of other Lu-pnictides, which are reported in Fig. 7a–d. The overall band structures from LuP to LuBi are quite similar to the electronic structure of LuN, with a small difference in detail. The DOS reported in Fig. 8a–d and the band structures as shown in Fig. 7, can be sub-divided into four regions separated by energy gaps. The bands in the lowest region around −10, −11, −9, and −11 eV for LuP, LuAs, LuSb, and LuBi, respectively, have mostly pnictogen *s* character with some amount of Lu *d* character mixed into them. The next four energy bands situated between −4 and −5 eV for LuP and LuAs, and −5 to −6 eV for LuSb and LuBi are Lu *f* bands with some contribution of Lu *d* and pnictogen *p* states. Bands just below the Fermi level are due to pnictogen *p* states with contribution of Lu *d* states. The unoccupied electronic states can be characterized as Lu *d* bands. The PDOS of these compounds in the B1 phase under ambient conditions is shown in Fig. 9a–d. We emphasize here that there are different distinct structures in the density of electronic states separated from each other by distinguishable gaps, confirming the band structures discussed above and showing clearly the contribution of the different states.

According to the present calculations, all the Lu-monopnictides are metallic except LuN, which is semiconducting in nature with an indirect band, gap of 1.55 eV. As

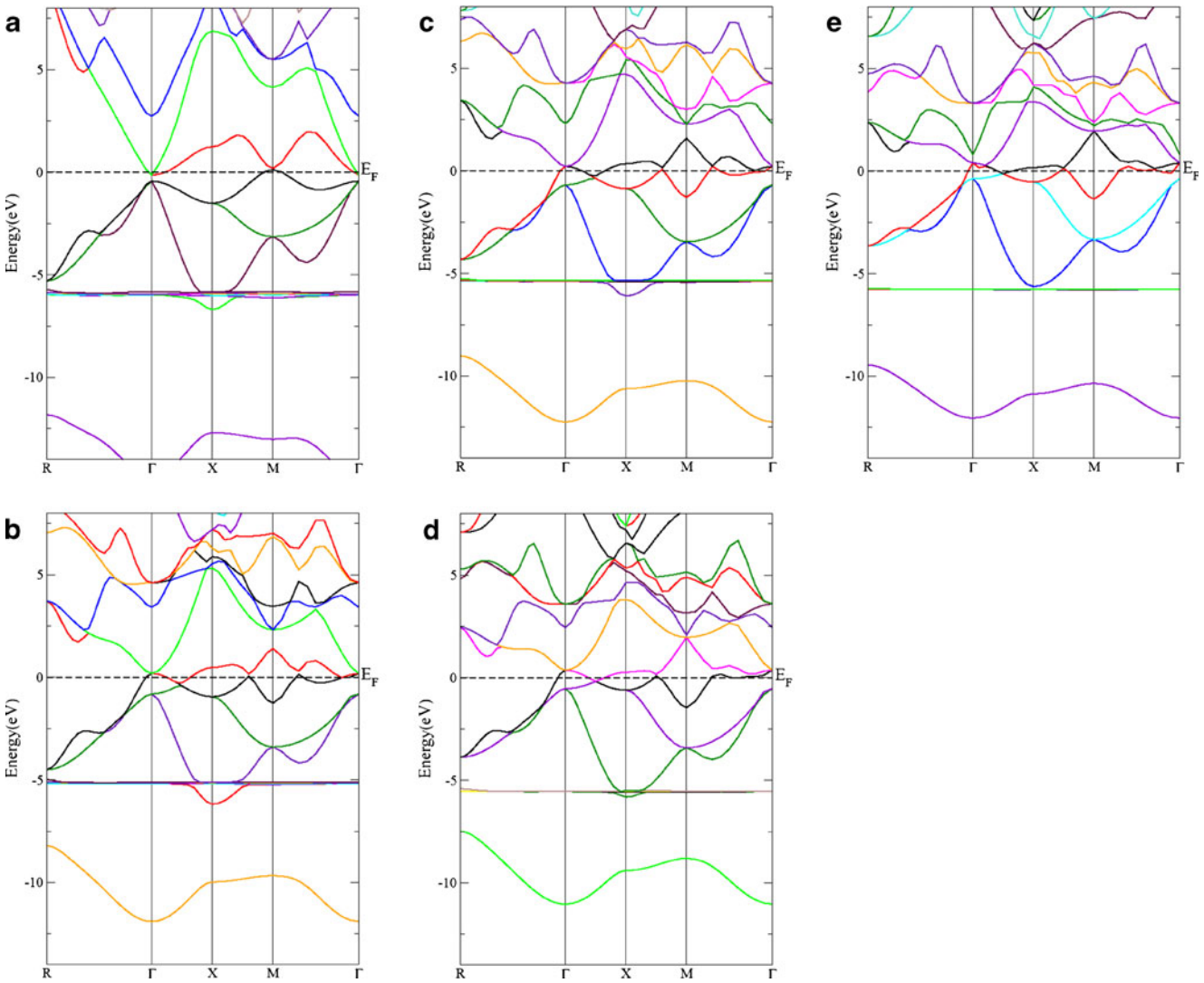

Fig. 10a–e Band structure for GGA + U in B2 phase just after the phase transition. **a** LuN, **b** LuP, **c** LuAs, **d** LuSb, **e** LuBi

LuP, LuAs, LuSb and LuBi are metallic in nature, hence the electronic structure reported here is by GGA + U only, because inclusion of SO simply show splitting among *f* bands only. The present results agree very well with experimental findings as well as earlier results.

To see the effect of high pressure on the electronic structure, we also computed the band structure and DOS (not reported here) in B2 phase (just after the B1→B2 transition) and plotted them in Fig. 10a–e. Figure 10a shows broadening in N-*p* states below the Fermi level and the splitting of unoccupied Lu-*d* states occur under pressure. Some of the N-*p* states below Fermi level and unoccupied Lu-*d* states cross Fermi level and show metallization. It is observed that other Lu-pnictides follow the same trend under pressure. Besides splitting of the unoccupied Lu-*d* states, band broadening can easily be observed in the *s* and *p* states of pnictogen atoms.

Conclusions

We performed ab-initio calculations of structural, elastic, thermal and electronic properties of Lu-pnictides in the B1 and electronic structure at high pressures B2 phases using GGA + U and GGA + (U-J) + SO methods. It was found that these materials are stable in B1 phase at ambient conditions. Under high pressure, Lu-pnictides transform from six-fold coordinated B1 phase to eight-fold coordinated B2 phase. The calculated lattice constants, bulk modulus and the first-order pressure derivatives of bulk modulus in B1 phase are in good agreement with experimental results. Our calculated elastic constants obey the traditional mechanical stability conditions for cubic crystals. The thermal properties for LuN, LuP, and LuBi compounds are reported for the first time. We also investigated the electronic structure of these materials in ambient conditions as well as at high pressures. Band structure of LuN, LuP, and LuBi and all Lu-pnictides (in B2 phase) are reported for the first time using effective on-site coulomb potential. The spin polarized GGA + (U-J) + SO scheme predicts a correct band gap value as compared to spin polarized GGA. We further point out that Coulomb repulsion (U) strongly influences the electronic structure of LuN, particularly in the treatment of correlation effects. Our results on Lu-pnictides are generally in good agreement with the available experimental data. These types of results are reported very scantily for RE monopnictides and hence requires more attention from researchers.

Acknowledgments The authors are thankful to the University Grants Commission (UGC), New Delhi (Govt. of India) for financial support.

References

1. Hullinger F (1979) In: Gchneidnet KA, Eyring L (eds) Handbook of physics and chemistry of rare earths, vol 4. North Holland, Amsterdam
2. Yakovkin IN, Komesu T, Dowben PA (2002) Phys Rev B66: 035406(1)–(8)
3. Lambrecht WRL (2000) Phys Rev B62:13538–13545
4. Leger JM (1993) Physica B190:84–91
5. Shirotani I, Yamanashi K, Hayashi J, Ishimatsu N, Shimomura O, Kikegawa T (2003) Solid State Commun 127:573–576
6. Errandonea D, Boehler R, Ross M (2000) Phys Rev Lett 85:3444–3447
7. Hayashi J, Shirotani I, Tanaka Y, Adachi T, Shimomura O, Kikegawa T (2000) Solid State Commun 114:561–565
8. De M, De SK (1999) J Phys Chem Solids 60:337–346
9. Sheng QJ, Cooper RR, Lim SP (1993) J Appl Phys 73:5409–5411
10. Li DX, Haga Y, Shida H, Suzuki T, Kwon YS (1996) Phys Rev B54: 10483–10491
11. Li DX, Haga Y, Shida H, Suzuki T, Kwon YS, Kubo G (1997) J Phys: Condens Matter 9:10777–10788
12. Tomimatsu T, Koyama K, Yoshida M, Li D, Motokawa M (2003) Phys Rev B67:014406(1)–(4)
13. Petukhov AG, Lambrecht WRL, Segall B (1996) Phys Rev B53: 4324–4339
14. Hasegawa A, Yanase A (1977) J Phys Soc Jpn 42:492–498
15. Liechtenstein AI, Antropov VP, Harmon BN (1994) Phys Rev B49: 10770–10773
16. Schoenes J, Repond P, Hullinger F, Lim SP, Cooper BR (1998) J Magn Magn Mater 177–181:1046–1047
17. Pagare G, Chouhan SS, Soni P, Sanyal SP, Rajagopalan M (2010) Comput Mater Sci 50:538–544
18. Chouhan SS, Pagare G, Soni P, Sanyal SP (2011) AIP Conf Proc 1349:97–98
19. Harima H, Kasuya T (1985) J Magn Magn Mater 52:370–372
20. Sj stedt E, Nordstrom L, Singh DJ (2000) Solid State Commun 114: 15–20
21. Blaha P, Schwarz K, Madsen GHK, Kuasnicka D, Luitz J (2001) WIEN2k an augmented plane wave+local orbitals program for calculating crystal properties. Technical Universitat Wien Austria ISBN 3-9501031-1-2
22. Perdew JP, Burke K, Ernzerhop M (1996) Phys Rev Lett 77:3865–3868
23. Anisimov VI, Solovyev IV, Korotin MA, Czyzyk MT, Sawatzky GA (1993) Phys Rev B48:16929–16934
24. Liechtenstein AI, Anisimov VI, Zaanen J (1995) Phys Rev B52: R5467–R5470
25. Madsen GHK, Novak P (2005) Euro Phys Lett 69:777–783
26. Monkhorst HJ, Pack JD (1976) Phys Rev B13:5188–5192
27. Sun Z, Li S, Ahuja R, Schneide JM (2004) Solid State Commun 129: 589–592
28. Jansiukiewicz C, Karpus V (2003) Solid State Commun 128:167–169
29. Wachter P, Filzmoser M, Rebizant J (2001) Physica B293:199–223
30. Duan CG, Sabirianov RF, Mei WN, Dowben PA, Jaswal SS, Tsymbal EY (2007) J Phys Condensed Matter 19:315220 (1–32)
31. Hayashi J, Shirotani I (2001) Memoirs Muroran Inst Technol 51: 191–199
32. Mehl MJ, Osburn JE, Papaconstantopoulous DA, Klein BM (1990) Phys Rev B41:10311–10323
33. Mehl MJ (1993) Phys Rev B47:2493–2500
34. Hill R (1952) Proc Phys Soc London A65:349–354
35. Gupta DC, Kulshrestha S (2011) J Alloys Compd 509:4653–4659
36. Pettifor DG (1992) Mater Sci Technol 8:345–349
37. Pugh SF (1954) Phil Mag 45:823–843